Clay Minerals (2023), **58**, 267–279
doi:10.1180/clm.2023.24

CAMBRIDGE UNIVERSITY PRESS

Article

Magnetic sepiolite/iron(III) oxide composite for the adsorption of lead(II) ions from aqueous solutions

Osman Uygun, Ayşenur Murat and Gaye Ö. Çakal
Institute of Nuclear Sciences, Ankara University, Beşevler, Ankara, Türkiye

Abstract

Clay minerals are effective adsorbents used for the remediation of toxic heavy metals from wastewater due to their large surface areas and great cation-exchange capacities. In this study, the removal of lead ions from aqueous solutions *via* adsorption was investigated using raw and iron-modified Turkish sepiolite. The aim of this study was to examine the effects of modification and environmental conditions on the sorptive properties of sepiolite samples. Initially, the raw sepiolite (Sep) and magnetic sepiolite/Fe_2O_3 composite (MagSep) prepared using the co-precipitation method were characterized *via* mineralogical and petrographical means and the physicochemical properties were determined. Then, the batch adsorption of lead (Pb^{2+}) ions on the sepiolite samples was examined under various conditions (solution pH, adsorbent dosage, contact time, initial Pb^{2+} ion concentration, temperature, shaking rate). The adsorption capacity of MagSep was found to be greater than that of Sep under all experimental conditions. The results showed that the adsorption process followed a pseudo-second-order kinetic model, and the Langmuir isotherm best correlated with the experimental data. The maximum adsorption capacities were found to be 60.6 and 90.1 mg g^{-1} for Sep and MagSep, respectively. The characterization of the Pb-adsorbed sepiolite samples showed that lead formed covalent bonds with the sepiolite samples and attached to the sepiolite surface mainly through ion exchange. MagSep can be used efficiently in the field of wastewater treatment for the removal of Pb^{2+} ions as it does not release any toxic pollutants and can be separated easily with the use of a magnetic field.

Keywords: Adsorption, characterization, lead, magnetic sepiolite, remediation, sepiolite

(Received 16 June 2023; revised 31 July 2023; accepted 17 August 2023; Accepted Manuscript online: 25 August 2023; Associate Editor: Chun Hui Zhou)

Heavy metals are highly toxic pollutants, with lead being one of the most frequently encountered. The main sources of lead are metal platings, fertilizers and pesticides, ore smelting, factory chimneys, vehicle exhaust fumes, urban waste and lead-based battery and paint products (Jaishankar *et al.*, 2014; Kumar *et al.*, 2022; Raj & Das, 2023). Environmental pollution occurs as a consequence of lead accumulation in air, water and soil. Living organisms are exposed to heavy metals through inhalation, ingestion or skin penetration. The damage to human health due to heavy metal exposure has been recognized previously (Deng *et al.*, 2022; Mitra *et al.*, 2022). When lead gets into the body, it generates reactive oxygen species, which lead to oxidative stress, causing cellular damage (Collin *et al.*, 2022). Lead interrupts physiological functions, encourages many respiratory syndromes and results in clinical disorders affecting the nervous, kidney, cardiovascular and other systems (Raj & Das, 2023). Hence, the levels of heavy metals in drinking water are limited by regulations and standards (Uddin, 2017; Tamjidi *et al.*, 2019); the level of lead is limited to 10 μg L^{-1} as stated by the World Health Organization (WHO) and the European Union (WHO, 2017; EU, 2020; Dettori *et al.*, 2022). This indicates the importance of the remediation of heavy metals from the environment.

Heavy metals have typically been removed from wastewater using the redox process, reverse osmosis, electrochemical treatment, bioremediation, coagulation, precipitation, ion exchange, membrane filtration and adsorption depending on the available budget and the initial heavy metal concentration (Rajendran *et al.*, 2022). Adsorption has become a popular method as its efficiency of removal can be improved with the development of original adsorbents and its cost is low compared to other separation processes (Fei & Hu, 2023). In adsorption, heavy metal ions in the aqueous solution attach successively to the surface of the adsorbent by means of physical or chemical interactions. The selection of the most efficient, easily accessible, low-cost, recyclable and environmentally friendly adsorbent is important to allaying environmental concerns (Novikau & Lujaniene, 2022). The ideal adsorbent should have a great accessible surface area (*via* a porous structure or small particle size), strong interaction between the active sites of the adsorbent and the heavy metals (employing surface modifications and/or optimum operating conditions), selectivity towards the targeted heavy metal species and easy regeneration (Fei & Hu, 2022).

Adsorbents are classified as carbon materials (activated carbon, carbon nanotubes, graphene and biochar), polymers (natural polymers such as chitosan and alginate, synthetic porous polymers such as amorphous porous organic polymers and crystalline

Corresponding author: Gaye Ö. Çakal; E-mail: gcakal@ankara.edu.tr
Cite this article: Uygun O, Murat A, Çakal GÖ (2023). Magnetic sepiolite/iron(III) oxide composite for the adsorption of lead(II) ions from aqueous solutions. *Clay Minerals* **58**, 267–279. https://doi.org/10.1180/clm.2023.24

covalent organic frameworks), metallic and metal compounds (nanoparticles, structurally engineered compounds and magnetic compounds) and others (minerals, boron and carbon nitrides, agricultural and industrial wastes and functionalized mesoporous adsorbents) according to their chemical components and material structures (Fei & Hu, 2022). From all of these, clay minerals are strong candidates for adsorption applications because of their global abundance, low cost and non-toxicity, in addition to their possession of a great surface area that enables the capture of cations and anions (Otunola & Olodale, 2020). For example, the use of bentonite, zeolite and perlite (Uygun *et al.*, 2023), kaolinite, montmorillonite, goethite and ferrihydrite (Mao *et al.*, 2023) and natural silicate minerals (Al-Degs *et al.*, 2003) for the adsorption of lead(II) has been reported previously. It should be noted that during the use of alumina-silicate minerals in wastewater treatments, these minerals may release Al into the solution (Uygun *et al.*, 2023).

Sepiolite, which has the chemical formula of $Si_{12}Mg_8O_{30}(OH)_4(OH_2)_4{\cdot}8H_2O$, is a natural, hydrated magnesium silicate clay mineral. It consists of a fibrous-like structure with fine microporous channels of various dimensions (Lazarević *et al.*, 2007; Dogan *et al.*, 2008). The structure of sepiolite is built up of ribbons of 2:1 layers, with each ribbon having a magnesium octahedral sheet between two layers of silica tetrahedra (Madejová *et al.*, 2017), which extend as a continuous layer with an inversion of the apical ends every six units. The ribbons are linked by the inversion of the SiO_4 tetrahedra through Si–O–Si bonds. This inversion produces a discontinuous octahedral sheet, in contrast to other clay minerals that contain continuous octahedral sheets. This gives sepiolite a structure with tunnel-like pores parallel to the fibre axis (Tartaglione *et al.*, 2008). Exchangeable cations of magnesium are located at the edges of the octahedral sheets, completing the coordinate number with two structural water molecules (bound water). This bound water is also connected to the zeolitic water by hydrogen bonds that fill the spaces in the channels (Mahmoud *et al.*, 2017). Previous studies have shown that sepiolite can remove toxic pollutants from the environment and retain a significant amount of heavy metal ions from aqueous solutions (Lazarević *et al.*, 2007). Brigatti *et al.* (1996) stated that heavy metal cation sorption can occur at the surface of broken edges, in channels and at specific sites of sepiolite according to crystal–chemical affinity. The adsorption of NH_3, H_2S and SO_2 (Zhou *et al.*, 2023), ethylene gas (Erdoğan & Esenli, 2021), phenanthrene (González-Santamaría *et al.*, 2017), Ni^{2+} ions (Kıpçak *et al.*, 2020) and red dye (Çoruh *et al.*, 2011) on sepiolite have also been reported previously.

The adsorption capacity of raw minerals can be improved through modifications, such as thermal, acid, organic and nano-zero-valent iron treatments, which increase their cation-exchange capacity (CEC) and surface area, resulting in increased adsorption capacity (Otunola & Olodale, 2020). The adsorption of various ions on sepiolite after acid treatment (Lazarević *et al.*, 2007), iron impregnation (Yu *et al.*, 2016; Fayazi *et al.*, 2019) and chemical modification (Dogan *et al.* 2008; Liang *et al.* 2013) has been studied previously in the literature. With the incorporation of iron, the minerals gain magnetic properties, and the combination of adsorption and magnetic properties makes adsorbents potentially applicable in wastewater treatment due to their ease of separation (Tamjidi *et al.*, 2019). The magnetic modification of chitosan (Wang *et al.*, 2023), biogas slurry solids (Sasidharan & Kumar, 2022), activated carbon (González Vázquez *et al.*, 2016) and mesoporous secondary nanostructures (Bhattacharya *et al.*, 2015) has also been reported previously.

Türkiye has 13.5 million tonnes of sepiolite reserves (OIK, 2018), and 4.53% (612,000 tonnes) of this reserve is in the Eskişehir region. A few studies have reported previously on the adsorption of Ni^{2+} (Kıpçak *et al.*, 2020), Cu^{2+} (Doğan *et al.*, 2009), Mn^{2+}, Cr^{3+} and Cd^{2+} (Kocaoba, 2009), Pb^{2+} (Bektaş *et al.*, 2004) and Co^{2+} (Kara *et al.*, 2003) using Turkish sepiolite. However, no study in the literature has reported the adsorption of Pb^{2+} using a magnetic sepiolite composite prepared from the sepiolite supplied from the Eskişehir region of Türkiye. Therefore, the aims of this study were: (1) to modify the surface of raw sepiolite supplied from Eskişehir, Türkiye, with iron; (2) to characterize both raw and modified sepiolite samples in detail; (3) to study the adsorption of Pb^{2+} ions from the aqueous solution using these sepiolite samples to observe the effects of surface modification on Pb^{2+} adsorption; (4) to fit the experimental data using various kinetic and adsorption isotherm models; (5) to discuss the adsorption mechanism of Pb^{2+} ions on the adsorbents; and (6) to characterize the adsorbents after Pb^{2+} ion adsorption.

Materials and methods

Materials and reagents

Raw sepiolite (Sep), supplied from Eskişehir, Türkiye, was first treated to remove the water-soluble impurities and organic matter and then sieved to obtain a particle size of <63 µm. $Pb(NO_3)_2$ (≥99.0% purity, Sigma-Aldrich), $Fe(NO_3)_3{\cdot}9H_2O$ (≥98% purity, Sigma-Aldrich) and all of the other chemicals used in this study were purchased as analytical grade.

Preparation of the magnetic sepiolite/Fe_2O_3 composite

The magnetic sepiolite/Fe_2O_3 composite (MagSep) was prepared using a procedure similar to that reported previously by Huang *et al.* (2017). Raw Sep was washed with Milli-Q® water and dried at 100°C in an oven to remove any impurities. To obtain MagSep, 7.05 g dry sepiolite was added to 300 mL Milli-Q water in a beaker, and the beaker was placed in an ultrasonic bath at room temperature. After dispersing the sepiolite fibres in water for 30 min, 16.16 g $Fe(NO_3)_3{\cdot}9H_2O$ was added to the water-bearing sepiolite and left in the ultrasonic bath for 1 h. To co-precipitate iron and the sepiolite, 10 M NaOH was droppered into the beaker until the pH equalled 10.0, and this was again kept in an ultrasonic bath for 1 h. The composite was then heated to 90°C and left in the ultrasonic bath for an additional 2 h. It was then left for 12 h at room temperature and washed with Milli-Q water until the pH equalled 7.0, and this was then centrifuged. Later, the composite was washed with ethanol and filtered. Finally, the MagSep was dried in an oven at 80°C for 4 h. The preparation process of MagSep is shown in Fig. 1a.

Characterization of Sep and MagSep

Mineralogical and petrographic analyses. X-ray diffraction (XRD) analysis of the sepiolite samples was performed using an Inel Equinox 1000 XRD spectrometer equipped with a Co X-ray tube. XRD traces were recorded at 5–70°2θ at a step size of 0.02°. The elemental analysis of samples was performed using a PANalytical Epsilon Model 1 X-ray fluorescence (XRF) spectrometer instrument according to the TS EN 15309 standard. Images and the elemental composition of the samples were obtained using scanning electron microscopy (SEM)/energy-dispersive spectroscopy (EDS) with a ZEISS EVO 40 apparatus. The infrared spectra of the sepiolite samples were recorded in the 4000–400 cm^{-1} region on a Varian/660-IR Fourier-transform infrared

https://doi.org/10.1180/clm.2023.24 Published online by Cambridge University Press

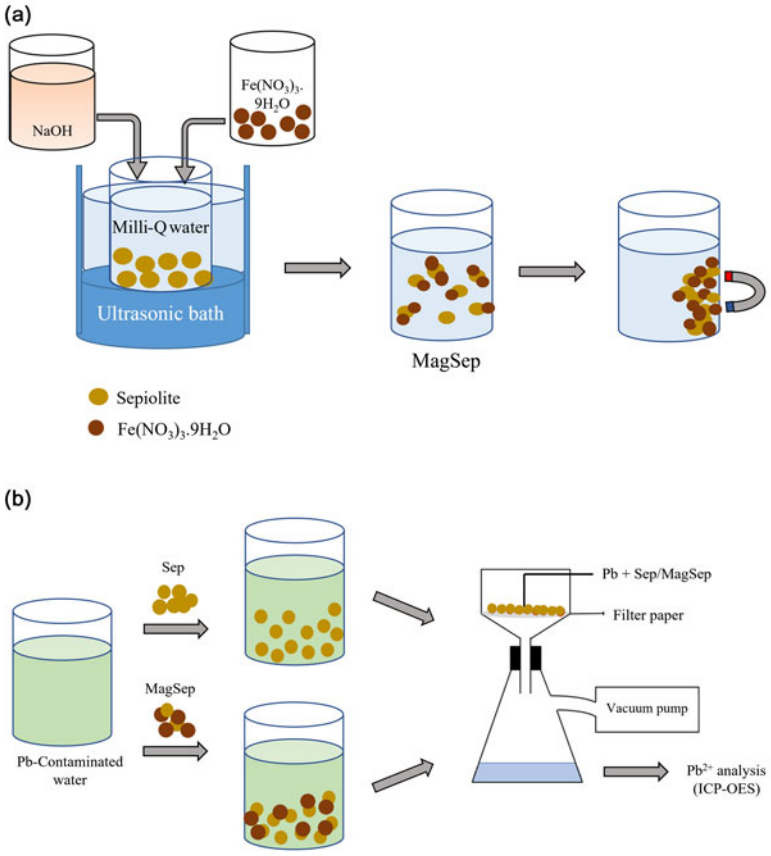

Figure 1. Schematic diagram of (a) MagSep synthesis and (b) Pb(II) adsorption on the sepiolite samples.

(FTIR) spectrometer. The XRF, SEM-EDS and FTIR analyses of the adsorbents were conducted after the adsorption experiments.

Physicochemical properties of the sepiolite samples

The water-absorption capacity, CEC, dissolution in water and point of zero charge (PZC) values of the sepiolite samples were determined as explained in detail in a previous study (Uygun *et al.*, 2023).

Specific surface area and Sauter mean particle diameter

The specific surface area and Sauter mean particle diameter of the sepiolite samples were determined using a Malvern Mastersizer 3000E device. The samples were dispersed in water and the measurements were performed at a stirring speed of 500 rpm.

Brunauer–Emmett–Teller surface area

The Brunauer–Emmett–Teller (BET) surface areas of the sepiolite samples were determined using a Quantachrome Autosorb 6B device.

ζ-potential

The ζ-potential values of the samples were determined at pH 7 using a Malvern Zetasizer Nano ZS90 device.

Vibrating-sample magnetometer analysis

The magnetic property of MagSep was determined using a Cryogenic Ltd PPMS device in vibrating-sample magnetometer (VSM) mode.

Batch adsorption experiments

The adsorption experiments of lead-contaminated waters were performed in 50 mL glass bottles according to ASTM 4646-03 (2004) to determine the effects of the initial pH (pH_i) value of the solution (3.0–9.0), adsorbent dosage (1–10 g L^{-1}), initial Pb^{2+} ion concentration (100–800 ppm), temperature (25–60°C), contact time (15–1440 min) and shaking rate (0–300 rpm). The effect of pH was examined by dispersing 0.25 g of adsorbent in a 50 mL Pb^{2+} solution at a concentration of 200 ppm. The pH_i value of the solution was adjusted *via* the addition of 1.0 M HCl or 1.0 M NaOH solution. The effect of the shaking rate was determined using an orbital shaking incubator (Mipro MLI-120). After the batch adsorption experiments, the filtrate was separated from the adsorbent using filter paper and the Pb^{2+} concentration in the filtrate was determined using inductively coupled plasma optical emission spectroscopy (ICP-OES). A schematic diagram showing the batch adsorption experiments is given in Fig. 1b. Reproducibility experiments were also performed, and differences in Pb^{2+} ion concentrations under the same experimental conditions were ~5%.

The adsorption capacity (q_t, mg g^{-1}), removal rate (R, %) and distribution coefficient (K_d, mL g^{-1}) were calculated using Equations 1–3, respectively:

$$q_t = (C_0 - C_t)\frac{V}{M} \quad (1)$$

$$R = \frac{C_0 - C_t}{C_0}100 \quad (2)$$

$$K_d = \frac{(C_0 - C_t)\,V}{C_t M} \quad (3)$$

https://doi.org/10.1180/clm.2023.24 Published online by Cambridge University Press

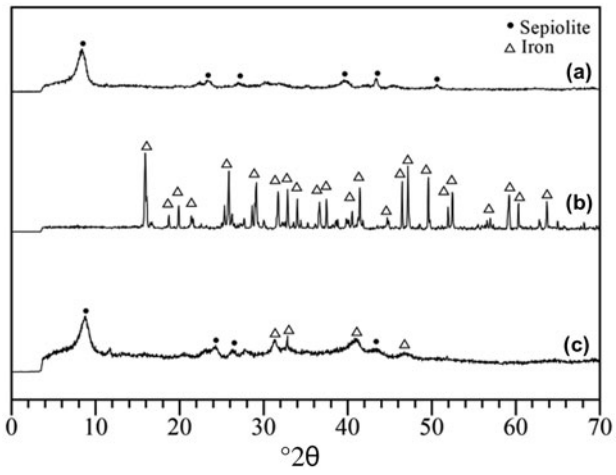

Figure 2. XRD spectra of (a) Sep, (b) $Fe(NO_3)_3{\cdot}9H_2O$ and (c) MagSep.

where C_0 is the initial mass concentration of the adsorbate (mg L^{-1}), C_t is the mass concentration of the adsorbate at any time t (mg L^{-1}), V is the volume of the aqueous solution (L), M is the mass of the adsorbent (g) and $q_t = q_e$ at $C_t = C_e$, with q_e and C_e denoting the equilibrium adsorption capacity and equilibrium mass concentration, respectively.

Adsorption kinetics were investigated using three different models: the pseudo-first-order model, pseudo-second-order model and intra-particle diffusion model. Adsorption isotherms were determined using the Langmuir and Freundlich equations. The thermodynamic parameters such as Gibbs free energy of adsorption ($\Delta G°$), heat of adsorption ($\Delta H°$) and entropy change ($\Delta S°$) related to the adsorption of Pb^{2+} ions on sepiolite samples were evaluated using Equations 4 and 5 and plotting $\ln(K_d)$ *vs* $1/T$ graphs:

$$\ln(K_d) = \frac{\Delta S^\circ}{R} - \frac{\Delta H^\circ}{RT} \quad (4)$$

$$\Delta G^\circ = \Delta H - T\Delta S = -RT\ln(K_d) \quad (5)$$

where T is temperature in Kelvin and R is the universal gas constant (8.314 J mol^{-1} K^{-1}).

Results and discussion

Mineralogical and petrographic characterization of the sepiolite samples

XRD spectra of sepiolite samples and $Fe(NO_3)_3{\cdot}9H_2O$ were acquired to examine the crystal structure of the Sep and MagSep samples (Fig. 2). It can be seen that the XRD spectrum of Sep (Fig. 2a) has peaks belonging only to sepiolite, whereas MagSep (Fig. 2c) has peaks related to the addition of iron (Fig. 2b), which demonstrated the incorporation of iron into the crystal structure of the Sep.

Although the chemical composition of sepiolite may vary according to its origin, the main constituents persist as silicate, magnesium and calcium oxides. The elemental compositions of the sepiolite samples used in this study were determined using XRF (Table 1). The main components of Sep were Si and Mg, whereas the main components of MagSep were Si and Fe. The Si contents of Sep and MagSep were 29.89% and 20.72%, respectively, and the Mg contents were 16.62% and 0.40%, respectively. As can be seen from Table 1, Mg was replaced by Fe (24.07%) in MagSep. The removal of Mg cations from the edges of the octahedral layers with iron coating has also been reported previously (Eren & Gumus, 2011).

SEM images of the sepiolite samples are shown in Fig. 3. Sep showed a fibrous-like structure, with the fibres having a high length to diameter ratio, whereas this structure can be seen to be altered significantly in the MagSep images (Fig. 3). Although fibres can also be observed in the MagSep images, a more porous structure was obtained due to the structural change of the dispersed sepiolite fibres and the modification of the surface with iron(III) nitrate during MagSep synthesis. The results of the EDS analyses of samples are presented in Fig. 4 together with the elemental distributions and compositions of the samples as insets. The presence of iron can be determined from the 6.5 keV peak, which corresponds to 43.68% iron in the MagSep sample. In addition, the silica and magnesium contents of MagSep were lower than those of the Sep sample, which was also observed from the XRF data (Table 1).

The FTIR spectra of Sep, $Fe(NO_3)_3{\cdot}9H_2O$ and MagSep were recorded in the 4000–400 cm^{-1} region (Fig. 5). In both the Sep and MagSep spectra, vibrations of the Mg–OH group were observed at 3690 cm^{-1} and coordinated water at 3566 cm^{-1} (Lazarević *et al.*, 2010). The peaks at 1660 cm^{-1} (Sep) and 1654 cm^{-1} (MagSep) corresponded to OH stretching vibrations, representing zeolitic water in the channels (Doğan *et al.*, 2008; Lazarević *et al.*, 2010) and bound water coordinated to magnesium in the octahedral sheet (Doğan *et al.*, 2008). The band at 1460 cm^{-1} was due to the hydroxyl bending vibration, which reflects the presence of bound water (Doğan *et al.*, 2008). The bands at 1210, 1080 and 970 cm^{-1} in the FTIR spectra of Sep and MagSep represented the stretching of Si–O bonds (Doğan *et al.*, 2008; Lazarević *et al.*, 2010; Ahribesh *et al.*, 2017), and the band at 1015 cm^{-1} exhibiting the Si–O–Si plane vibrations was due to the basal plane of the tetrahedral units (Tabak *et al.*, 2009). There were bands at 690 and 640 cm^{-1}, corresponding to the vibrations of the Mg–OH bond, and a band at 460 cm^{-1} originating from octahedral–tetrahedral bonds (Si–O–Mg bonds; Lazarević *et al.*, 2010).

Table 1. Elemental compositions (wt.%) of sepiolite samples before and after Pb^{2+} adsorption experiments as obtained from XRF.

Adsorbent		Na	Mg	Al	Si	K	Ca	Fe	Pb	LOI
Sep	Before adsorption	0.02	16.62	0.01	29.89	0.23	0.86	0.18	–	6.73
	After adsorption	0.05	9.17	–	19.93	0.29	0.72	0.20	3.12	
MagSep	Before adsorption	0.05	0.40	0.49	20.72	0.11	0.31	24.07	–	18.73
	After adsorption	0.07	1.04	0.22	5.12	0.18	0.24	17.33	5.49	

LOI = loss on ignition.

https://doi.org/10.1180/clm.2023.24 Published online by Cambridge University Press

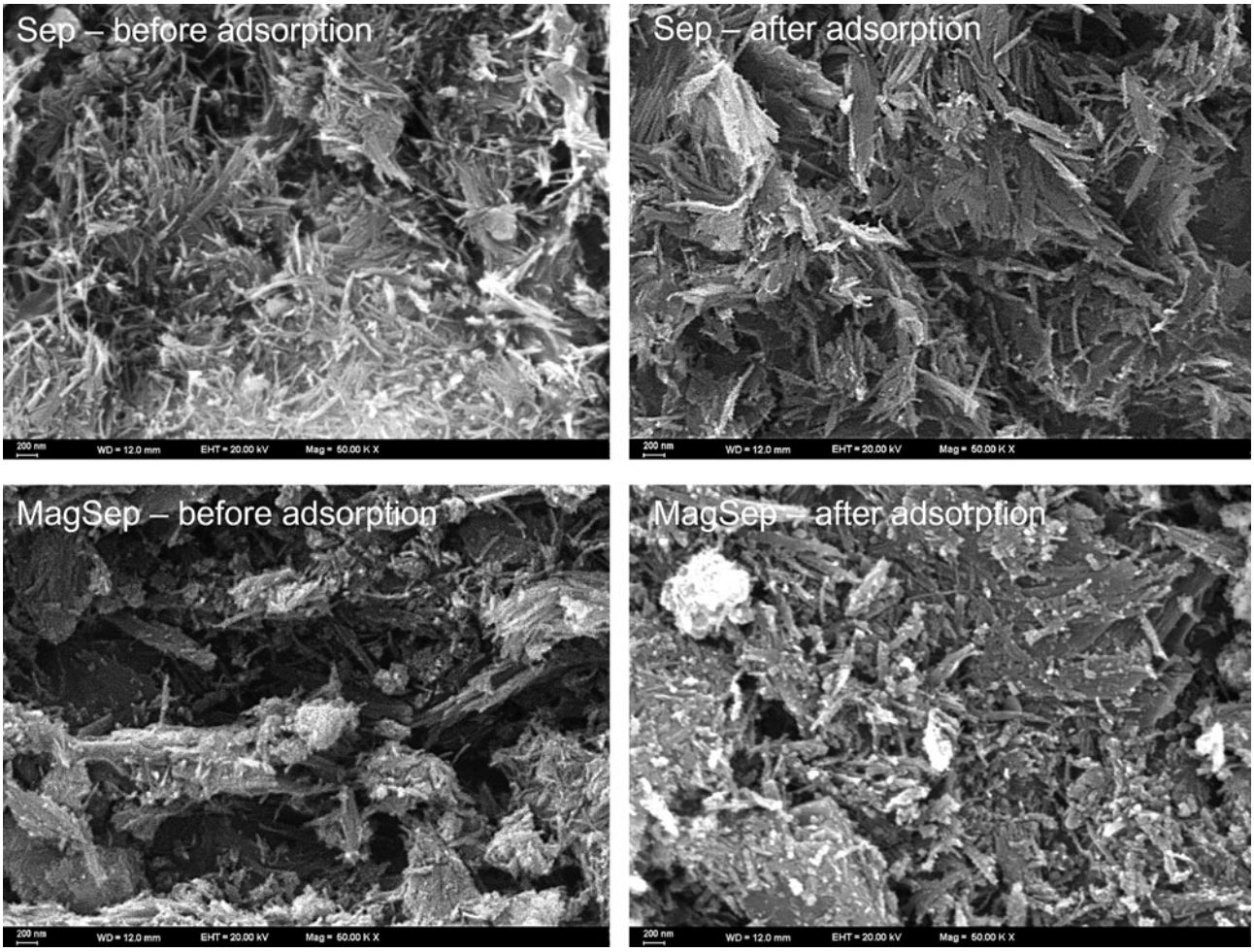

Figure 3. SEM images of Sep and MagSep before and after Pb^{2+} adsorption.

The band at 2394 cm^{-1} in the spectrum of iron nitrate appeared at 2350 cm^{-1} in the spectrum of MagSep, indicating a chemical interaction with iron occurring on the sepiolite surface during the modification. There was also a weak band at 1750 cm^{-1} in the FTIR spectrum of MagSep and iron nitrate, which could be due to the stretching of Fe–OH groups. In addition, the shift of the 1660 cm^{-1} band (Sep) to 1654 cm^{-1} (MagSep) and the 1460 cm^{-1} band (Sep) to 1416 cm^{-1} (MagSep) demonstrated the decrease in H_2O content with the replacement of iron oxide molecules (Eren & Gumus, 2011). Thus, it can be stated that a successful surface modification of sepiolite was achieved and iron oxide was integrated into the sepiolite structure, forming covalent bonds between iron oxide and sepiolite.

Physicochemical properties of the sepiolite samples

The physicochemical properties of the sepiolite samples are presented in Table 2. The average particle size of Sep was 20.4 μm, which increased to 328.0 μm (MagSep) after the surface modification (Fig. 6). It can be seen that the number of particles with greater particle sizes increased after the modification. Thus, the specific surface area of Sep was reduced by 16 times in MagSep.

The great water-absorption capacities and low dissolution percentages make these sepiolite samples preferable materials for various areas of application such as wastewater remediation. From the results (Table 2), it can be said that the surface modification process decreased the water-absorption capacity of sepiolite by ∼10%, and the dissolution percentage of sepiolite decreased by 51%, leading to less contamination of the treated water. The dissolved ions in the water were determined using ICP-OES analysis, and the data are presented together with the elemental analysis of Milli-Q water in Table 3 for comparison.

The ions that were most dissolved were Ca in Sep and Na in MagSep. Although Na was not present in great amounts in Sep (Table 1), the presence and dissolution of Na in water were due to the use of NaOH to attain a high pH while preparing the MagSep sample. It should also be mentioned that the ions released into the water are not toxic to the environment, which is an important concern relating to the pollution of remediated water sources. Iron is also included in Table 3 to demonstrate that iron was not dissolved after the surface modification as it was chemically bound to the surface. The metal cations occupy various positions inside the mineral, and their release depends on their structural positions. When they are weakly bonded inside the channels or on the mineral surfaces, they are partly but very rapidly released, whereas at the channel edges in the octahedra, they are bonded more strongly with similar exchange cations (Brigatti *et al.*, 1996).

The BET surface area and CEC of the materials are the main physicochemical properties used for the selection of an adsorbent. The BET surface area of Sep was found to be 352.46 $m^2\ g^{-1}$, which

https://doi.org/10.1180/clm.2023.24 Published online by Cambridge University Press

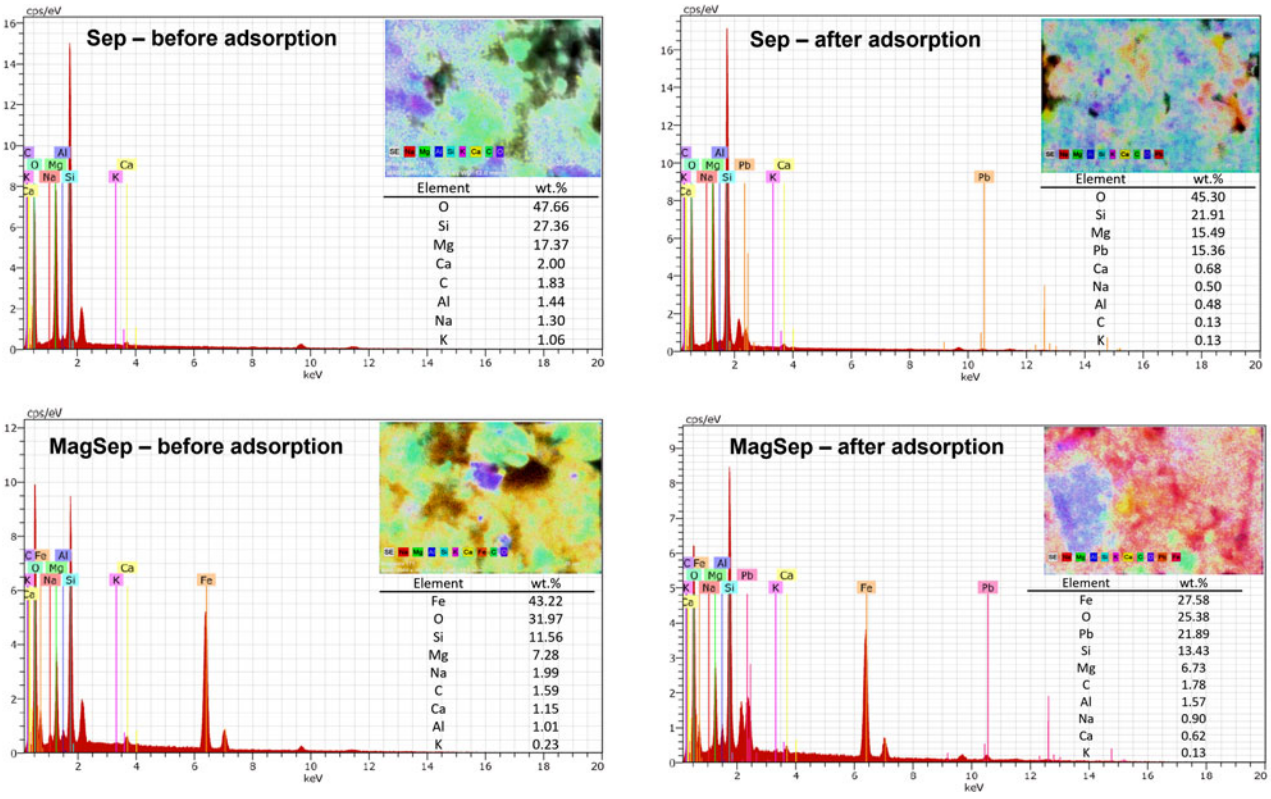

Figure 4. EDS analyses of Sep and MagSep before and after Pb^{2+} adsorption. Insets show the elemental distributions and compositions of the samples.

was comparable to the results obtained in studies performed using sepiolite supplied from Eskişehir, Türkiye (Doğan *et al.*, 2008). The BET surface area of MagSep was found to be 9% lower than that of Sep (Table 2), which was due to the alteration of the fibrous-like structure of the sepiolite after surface modification by iron. The CEC of MagSep was doubled for the same reason. In the literature, the CEC of sepiolite has been reported to be between 10 and 45 meq 100 g^{-1} (Christidis, 2011).

VSM analysis was performed to determine whether the synthesis of MagSep was successful in terms of achieving magnetic properties. The magnetization curve of the MagSep sample is shown in Fig. 7. It can be seen that MagSep showed paramagnetic properties and the saturation value of magnetism was 0.5 emu g^{-1}. The inset image in Fig. 7 demonstrates the behaviour of MagSep under an external magnetic field. It can be concluded that MagSep can easily be separated from aqueous solutions using permanent powerful magnets when used as an adsorbent.

Batch adsorption experiments

The effect of the pH_i of the solution on Pb^{2+} adsorption on sepiolite samples. pH_i is the most important parameter regarding adsorption as pH affects both the formation of lead compounds and the surface charge of the adsorbent. The effect of the pH_i on the adsorption of Pb^{2+} ions in the contaminated aqueous solution by sepiolite samples was investigated in the pH range of 3.0–9.0 at 25°C for 1440 min, an initial Pb^{2+} ion concentration of 200 ppm, a shaking rate of 75 rpm and an adsorbent dosage of 5 g L^{-1}.

The removal percentage of Pb^{2+} using Sep was lower compared to MagSep until pH = 7.0 and then equal at pH 7.0–9.0 (q = 39.9 mg g^{-1}; Fig. 8). The adsorption capacity of the sepiolite modified by Fe_3O_4 and MnO_2 was found to be equal to ~50 mg g^{-1} at pH 6-9 (Fayazi *et al.*, 2019). The low removal percentages at low pH values (pH < PZC) can be attributed both to the positive charge density on the surface sites of sepiolite minerals that causes electrostatic repulsion between Pb^{2+} ions and the edge groups with positive charge (Si–OH^{2+}) on the surface of sepiolite particles, and to the excess amount of H_3O^+ ions in the solution, which compete with the positively charged H^+ ions and Pb^{2+} ions for the available adsorption sites on the sepiolite surface (Sharifipour *et al.*, 2015). Hence, the pH_i of the solution was taken as 7.0 in all of the batch adsorption experiments.

The ζ-potentials of Sep and MagSep, showing the potential difference between the dispersion medium and the stationary layer of the fluid of the sepiolite sample, at pH 7.0 were found to be –17.2 and –27.0 mV, respectively (Table 2). It can also be deduced from the Pourbaix diagram of lead that Pb(II) exists as a cation at pH 7.0 (Lehto & Hou, 2010). Thus, the removal of lead can be caused by the electrostatic attraction between the negatively charged sepiolite surface and the positively charged Pb^{2+} ions. In addition, the main mechanism for the adsorption of divalent cations on sepiolite powder is the ion exchange of Mg^{2+} ions from the sepiolite structure with metal ions (M^{2+}) from the solution (Lazarević *et al.*, 2007). This suggests that the retention of Pb^{2+} ions on the sepiolite sample surfaces took place through electrostatic interaction and exchange of Mg^{2+} ions together. The affinity for ion exchange being greatest in the case of Pb^{2+} ions was also reported by Lazarević *et al.* (2007).

The effect of contact time on Pb^{2+} adsorption on the sepiolite samples/adsorption kinetics

To investigate the effect of contact time on adsorption, experiments were carried out for 15–1440 min at pH 7.0, temperature

https://doi.org/10.1180/clm.2023.24 Published online by Cambridge University Press

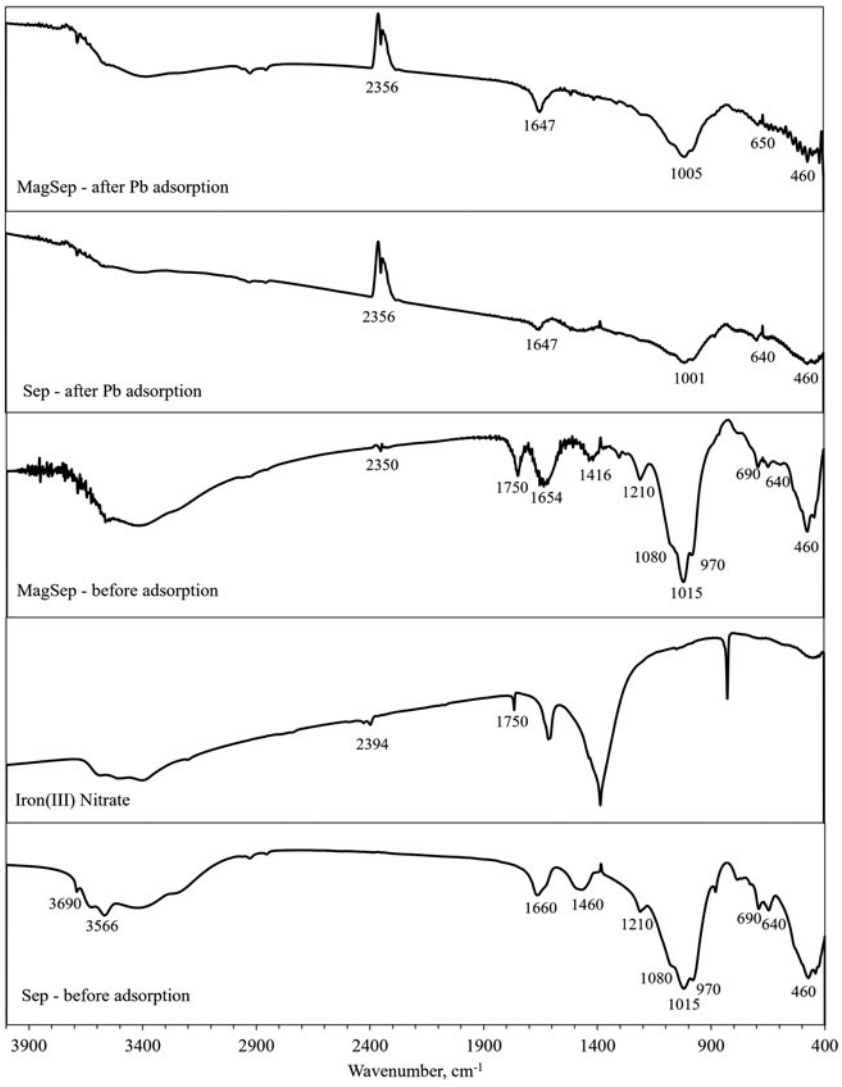

Figure 5. FTIR spectra of Sep, $Fe(NO_3)_3{\cdot}9H_2O$ and MagSep before and after Pb^{2+} adsorption.

25°C, an initial Pb^{2+} ion concentration of 400 ppm, a shaking rate of 75 rpm and an adsorbent dosage of 5.0 g L^{-1}. The removal percentages as a function of time are shown in Fig. 9a.

It was observed that the adsorption of lead ions on the sepiolite samples was completed at nearly 2 h for both samples. It can be said that the adsorption capacity increased by 2.35 mg g^{-1} (5.25%) with contact time when the adsorption capacity at 2 h was compared with 24 h. Hence, the remainder of the adsorption experiments were performed at 2 h. MagSep showed greater adsorption capacities at each studied contact time. Lead removal of 74.86% was achieved at 2 h, which was 21.72% greater than Sep, demonstrating the increase in adsorption performance with surface modification.

In a previous study, the adsorption of lead was studied under similar experimental conditions, and the adsorption capacities were in the following order: bentonite > zeolite > perlite (Uygun *et al.*, 2023). When the removal percentages of Sep and

Table 2. Physicochemical analysis of Sep and MagSep.

Physicochemical property	Sep	MagSep
Mean particle size (μm)	20.4	328.0
Specific surface area (m^2 g^{-1})	0.294	0.018
Water-absorption capacity (%)	75.34	64.77
Dissolution (%)	6.77	3.31
BET surface area (m^2 g^{-1})	351.46	319.67
CEC (meq 100 g^{-1})	15.6	31.2
PZC	5.66	5.64
ζ-potential (pH = 7)	−17.2	−27.0

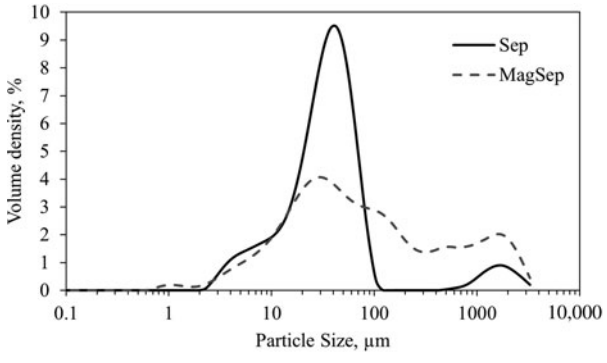

Figure 6. Particle-size distribution of the sepiolite samples.

https://doi.org/10.1180/clm.2023.24 Published online by Cambridge University Press

Table 3. Elemental analysis of dissolved elements in the sepiolite samples (ppm).

Sample	Na	Mg	K	Ca	Fe
Sep	0.70	0.70	0.22	2.31	0.07
MagSep	16.07	0.29	0.33	0.57	0.03
Milli-Q	0.73	0.03	0.00	0.03	0.07

MagSep at 2 h were compared with these minerals, the new order became: bentonite (95%) > MagSep (75%) > Sep (53%) > zeolite (42%) > perlite (27%). This demonstrates that bentonite has a greater affinity for lead ions.

Adsorption kinetics were studied to investigate the dependence on the physical and/or chemical characteristics of the sepiolite samples and thus the influence of contact time on the adsorption mechanism. The mechanism of adsorption was examined from the linear fitting of the kinetic data to the pseudo-first-order, pseudo-second-order and intra-particle diffusion models (Fig. 9b). The kinetic equations of the corresponding models are given in Table 4.

The rate constants (k_1, k_2, k_3) were determined from the slopes, and the equilibrium adsorption capacities (q_e) and intra-particle diffusion model constants (b) were determined from the intercepts of the linear equations (Fig. 9b & Table 4). It can be seen that lead adsorption was a time-dependent process and that the adsorption of Pb^{2+} on the sepiolite samples conformed with the second-order kinetic model ($R^2 = 0.9999$ for Sep and 0.9995 for MagSep). The equilibrium adsorption capacities (q_e) found from the model were also comparable (~3% difference) to the adsorption capacities found experimentally at 1440 min. Previous studies investigating the adsorption of lead on raw Sep (Bektaş *et al.*, 2004; Sharifipour *et al.*, 2015), Fe_2O_3–MnO_2-modified sepiolite (Fayazi *et al.*, 2019) and mercapto-functionalized sepiolite (Liang *et al.*, 2013) have also reported that the experimental data conformed to pseudo-second-order kinetics.

The effect of adsorbent dosage on Pb^{2+} adsorption on the sepiolite samples

The effect of adsorbent dosage on the adsorption of Pb^{2+} from the contaminated aqueous solution by Sep and MagSep was studied by varying the adsorbent dosage between 1 and 10 g L^{-1} at pH 7.0, temperature 25°C, a contact time of 120 min, a shaking rate of 75 rpm and an initial Pb^{2+} ion concentration of 400 ppm (Fig. 10).

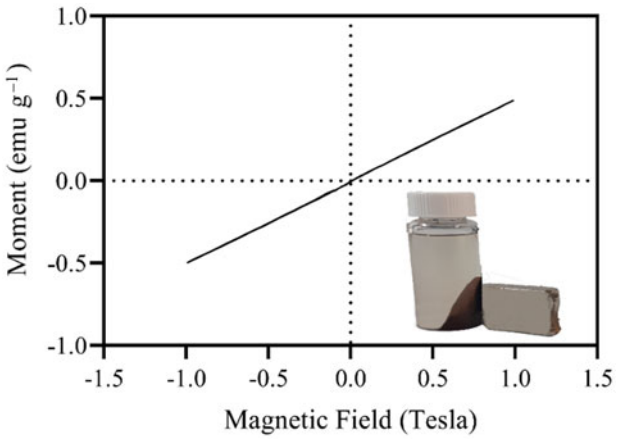

Figure 7. The magnetization curve of MagSep. The behaviour of MagSep under the influence of an external magnetic field is given in the inset image.

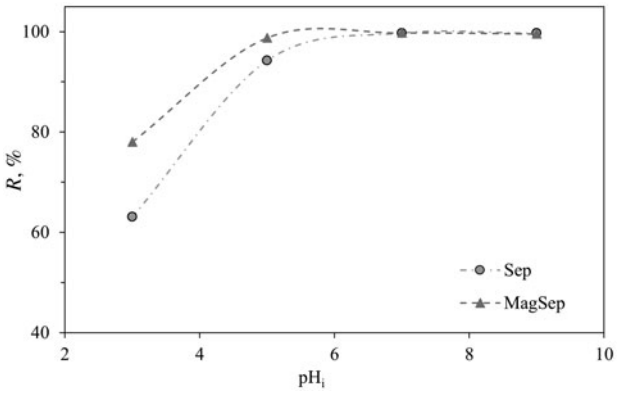

Figure 8. The effect of pH_i on the adsorption of Pb^{2+} by the sepiolite samples (adsorbent dosage = 5 mg L^{-1}, contact time = 1440 min, initial concentration of Pb^{2+} = 200 ppm, temperature = 25°C, shaking rate = 75 rpm).

It is clear that the removal percentage of Pb^{2+} ions increased with the adsorbent dosage, as more Pb^{2+} ions were adsorbed from the greater amount of active sites on the surface of the sepiolite samples. The maximum adsorption capacities were 94.85 and 175.32 mg g^{-1} at the adsorbent dosage of 1 g L^{-1} for Sep and MagSep, respectively, whereas the greatest removal percentages were achieved at the adsorbent dosage of 10 g L^{-1}, with values of 95.81% and 97.55% for Sep and MagSep, respectively. It was observed that the difference in adsorption capacities and, hence, the removal percentages between the two adsorbents decreased with increasing adsorbent dosages. The number of unsaturated adsorption sites on the adsorbent increased at high dosages, leading to a progressive decrease in adsorption capacities (Fayazi *et al.*, 2019). Considering both the adsorption capacities and removal percentages of the sepiolite samples, an adsorbent dosage of 5 g L^{-1} was selected for the remainder of the adsorption experiments.

The effect of initial Pb^{2+} concentration on Pb^{2+} adsorption on the sepiolite samples/adsorption isotherms

The effect of initial Pb^{2+} concentration on the adsorption of Pb^{2+} on the sepiolite samples was studied by varying the initial Pb^{2+} ion concentrations between 100 and 800 ppm at pH 7.0, temperature 25°C, a contact time of 120 min, a shaking rate of 75 rpm and an adsorbent dosage of 5 g L^{-1} (Fig. 11a).

There was no difference between the adsorption capacities of Sep and MagSep at the initial adsorbate concentrations (100–200 ppm), and the removal percentages were >99.5% (Fig. 11a). Moreover, the difference between the adsorption capacities, and hence the removal percentages, increased with increasing adsorbate concentrations. As predicted, MagSep showed greater adsorption capacities than Sep at increased adsorbate concentrations, with the difference being 17.49% at 800 ppm. Similarly, the adsorption capacity of MagSep was 89 mg g^{-1}, whereas it was 61 mg g^{-1} for Sep at the initial adsorbate concentration of 800 ppm. The increase in adsorption capacities with initial Pb^{2+} concentration is due to the fact that the mass transfer driving force would become larger at greater initial adsorbate concentrations (Fayazi *et al.*, 2019). It can be concluded that aqueous solutions of 400 ppm can be adsorbed by MagSep with a removal percentage of 74.86%.

https://doi.org/10.1180/clm.2023.24 Published online by Cambridge University Press

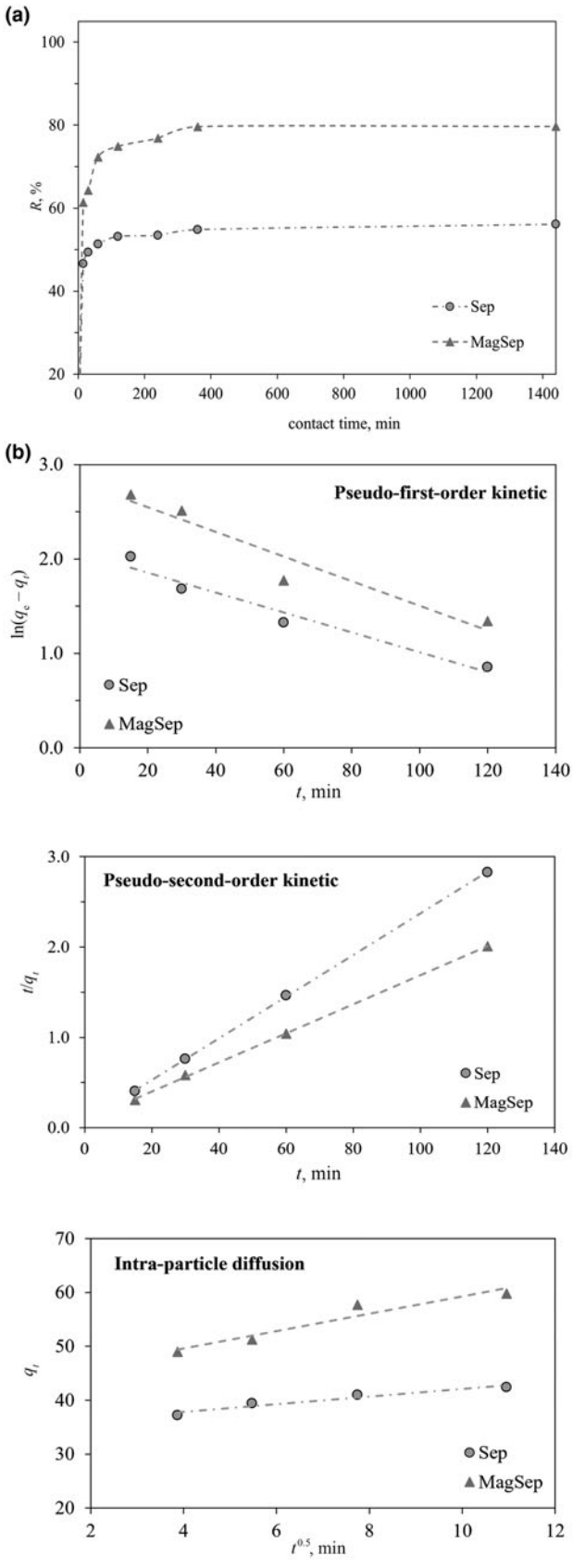

Figure 9. (a) The effect of contact time on the adsorption of Pb^{2+} by the sepiolite samples (pH = 7, temperature = 25°C, adsorbent dosage = 5 g L^{-1}, initial concentration of Pb^{2+} = 400 ppm, shaking rate = 75 rpm) and (b) the adsorption kinetic models.

The Langmuir and the Freundlich equations are often used to describe adsorption equilibria for wastewater treatment applications. The adsorption isotherm that best fit the experimental data was determined using the linear forms of these models (Fig. 11b). The equations of the corresponding isotherm models are shown in Table 5.

The maximum adsorption capacities (q_m) and Freundlich isotherm constants (n) were found from the slopes, and the Langmuir and Freundlich adsorption coefficients (K_L, K_F) were found from the intercepts of the corresponding linear equations (Fig. 11b & Table 5). By taking into account the correlation coefficients (R^2), it can be seen that the Langmuir isotherm showed a better correlation over the studied concentration range for all adsorbents (R^2 = 0.9718 for Sep and 0.9795 for MagSep). The maximum adsorption capacities (q_m) were determined as 60.6 and 90.1 mg g^{-1} for Sep and MagSep, respectively. As the Langmuir isotherm fit the experimental data, this denotes that the sepiolite samples had a homogeneous distribution of active sites, indicating that monolayer adsorption on the surface of the sepiolite samples was observed (Huang *et al.*, 2017). Previous studies investigating the adsorption of lead on raw and modified sepiolite have found that the data better fit the Langmuir isotherm (Bektaş *et al.*, 2004; Fayazi *et al.*, 2019) and Freundlich isotherm (Liang *et al.*, 2013).

Studies investigating the adsorption of lead on the sepiolite minerals also found the maximum adsorption capacities to be 31.5 mg g^{-1} (Sharifipour *et al.*, 2015), 51.36 mg g^{-1} (Eren & Gumus, 2011), 72.52 mg g^{-1} (Lazarević *et al.*, 2007) and 93.54 mg g^{-1} (Bektaş *et al.*, 2004) for raw Sep, 45.58 mg g^{-1} (Lazarević *et al.*, 2007) for acid-activated sepiolite and 75.79 mg g^{-1} (Eren & Gumus, 2011) and 131.58 mg g^{-1} (Fayazi *et al.*, 2019) for iron-modified sepiolite.

The effect of temperature on Pb^{2+} adsorption on the sepiolite samples/adsorption thermodynamics

The effect of temperature on the adsorption capacity of Pb^{2+} was studied at temperatures of 25–60°C at pH 7.0 for 120 min, an adsorbent dosage of 5 g L^{-1}, a shaking rate of 75 rpm and an initial Pb^{2+} ion concentration of 400 ppm. It was found that the removal percentages increased with temperature, with lead removal rates of 64% (51.52 mg g^{-1}) and 84% (67.23 mg g^{-1}) at 60°C for Sep and MagSep, respectively. As the adsorption capacities of both sepiolite samples increased with temperature, the adsorption of Pb^{2+} on the sepiolite samples can be explained by chemical adsorption on the active sites of the samples. This was supported by the Langmuir adsorption isotherm determined previously, as in this model the ions are adsorbed on the adsorbate *via* covalent bonds, which are difficult to break at temperatures <100°C. To obtain high removal percentages of lead ions, temperatures >45°C and surface modification with iron impregnation of sepiolite can be suggested.

The enthalpy change ($\Delta H°$) and entropy change ($\Delta S°$) were obtained from the slope and intercept of the Van 't Hoff plot (Fig. 12) using Equation 4, and the Gibbs free energy of adsorption ($\Delta G°$) was found from Equation 5.

The thermodynamic parameters of Sep and MagSep are listed in Table 6. Both Sep and MagSep showed a positive enthalpy change, demonstrating that the adsorption of lead ions on the sepiolite samples was endothermic. Furthermore, the observed enthalpy change was greater than that of typical ion-exchange reactions (typically <8.4 kJ mol^{-1}; Liang *et al.*, 2013), suggesting that specific interactions other than outer-sphere electrostatic interactions are operative in the Pb–sepiolite adsorption system.

https://doi.org/10.1180/clm.2023.24 Published online by Cambridge University Press

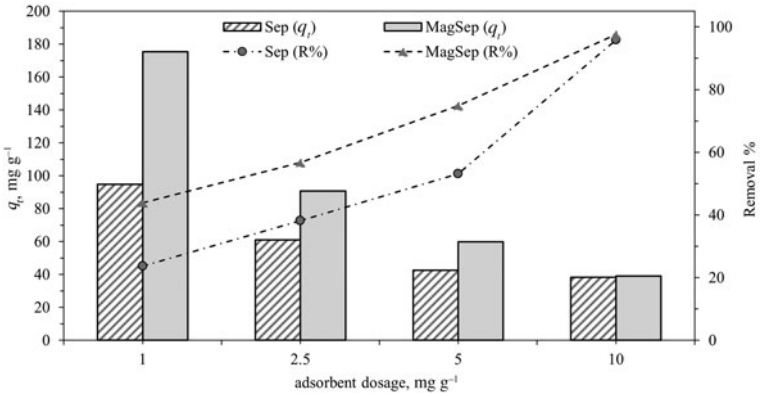

Figure 10. The effect of adsorbent dosage on the adsorption of Pb^{2+} by the sepiolite samples (pH = 7, contact time = 120 min, initial concentration of Pb^{2+} = 400 ppm, shaking rate = 75 rpm, temperature = 25°C).

Table 4. Kinetic models, model constants and coefficients of correlation (R^2) for the adsorption of Pb^{2+} ions on Sep and MagSep.

Kinetic model		Model constants[a]	Sep	MagSep
Pseudo-first order	Non-linear equation $q_t = q_e(1 - e^{-k_1 t})$ Linear equation $\ln(q_e - q_t) = \ln(q_e) - k_1 t$	k_1 (1 min^{-1})	0.0106	0.0130
		q_e (mg g^{-1})	7.91	16.61
		R^2	0.9570	0.9264
Pseudo-second order	Non-linear equation $q_t = \frac{k_2 q_e^2 t}{1+k_2 q_e t}$ Linear equation $\frac{t}{q_t} = \left(\frac{1}{k_2 q_e^2}\right) + \frac{t}{q_e}$	k_2 (g mg^{-1} min^{-1})	7.95×10^{-3}	3.19×10^{-3}
		q_e (mg g^{-1})	43.29	62.11
		R^2	0.9999	0.9995
Intra-particle diffusion	$q_t = k_3 t^{0.5} + b$	k_3 (mg g^{-1} min$^{-1/2}$)	0.7096	1.6047
		b (mg g^{-1})	35.03	43.19
		R^2	0.9379	0.9235

[a]k_1, k_2 and k_3 are the rate constants and b is the intra-particle diffusion model constant.

The negative values of the Gibbs free energy change for both sepiolite samples indicate that the adsorption process occurred spontaneously. The increasingly negative values of $\Delta G°$ with increasing temperature indicate that the adsorption reactions were more favourable thermodynamically at greater temperatures. Entropy change was positive for both adsorbents, reflecting an increase in randomness at the solid/liquid interface during the adsorption of Pb^{2+} on the sepiolite samples.

The enthalpy and entropy change of MagSep were greater than for Sep, while the reverse was true for Gibbs free energy change, leading to an increased adsorption capacity of MagSep compared to Sep (Table 6). Spontaneous and endothermic adsorption of lead on sepiolite samples has also been reported previously (Bektaş *et al.*, 2004; Eren & Gumus, 2011; Liang *et al.*, 2013; Fayazi *et al.*, 2019).

The effect of shaking rate on Pb^{2+} adsorption on the sepiolite samples

The effect of shaking rate on Pb^{2+} ion adsorption was studied by varying the shaking rate between 0 and 300 rpm at pH 7.0, temperature 25°C, a contact time of 120 min, an adsorbent dosage of 5 g L^{-1} and an initial Pb^{2+} ion concentration of 400 ppm. It was found that the adsorption capacities of Sep and MagSep were comparable until 150 rpm, after which a steep increase was observed at 300 rpm for both of the adsorbents. The removal percentages of Sep and MagSep were 50.55 ± 4.14% (40.44 ± 3.31 mg g^{-1}) and 70.93 ± 3.73% (56.40 ± 3.45 mg g^{-1}) for 0–150 rpm, whereas they were 91.46% (73.17 mg g^{-1}) and 94.88% (75.91 mg g^{-1}) at 300 rpm. It can be concluded that the adsorption capacities can be increased to a greater extent at greater shaking rates as there was a more homogeneous distribution of the adsorbents in the aqueous solution, which also increased the chance of lead ions binding to the active sites of the sepiolite surfaces.

Characterization of the sepiolite samples after Pb^{2+} ion adsorption

After the batch adsorption experiment at pH 7.0, a contact time of 120 min, an adsorbent dosage of 5 g L^{-1}, a shaking rate of 75 rpm and a temperature of 25°C using an initial Pb^{2+} ion concentration of 400 ppm, the adsorbed Pb^{2+} ions on the sepiolite samples were examined using XRF (Table 1), FTIR (Fig. 5) and SEM-EDS (Figs 3 & 4) analyses. It should be noted that the removal percentages of Pb^{2+} were found to be 53% and 75% for Sep and MagSep, respectively. The XRF analysis showed that Pb^{2+} was adsorbed successfully on the surfaces of Sep (3.12%) and MagSep (5.49%). The interaction between the surface of the sepiolite samples and Pb^{2+} ions can be argued to result from both electrostatic attraction due to the surface charge of the adsorbents and from ion exchange due to the exchange of cations, such as Mg and Ca. The decrease of Si after the adsorption (Table 1) also indicates the breakage of Si–O bonds during the adsorption process. The FTIR spectra (Fig. 5) show the changes in the positions and shapes of the fundamental vibrations of OH and Si–O groups due to the new Pb bonds formed. For example, the disappearing 1210 cm^{-1} band and the decreased intensity and the shift of the 1015 cm^{-1} band to 1001 cm^{-1} (Sep) and 1005 cm^{-1} (MagSep) indicate that Pb^{2+} ions influenced both Si–O bonds and Si–O–Si

https://doi.org/10.1180/clm.2023.24 Published online by Cambridge University Press

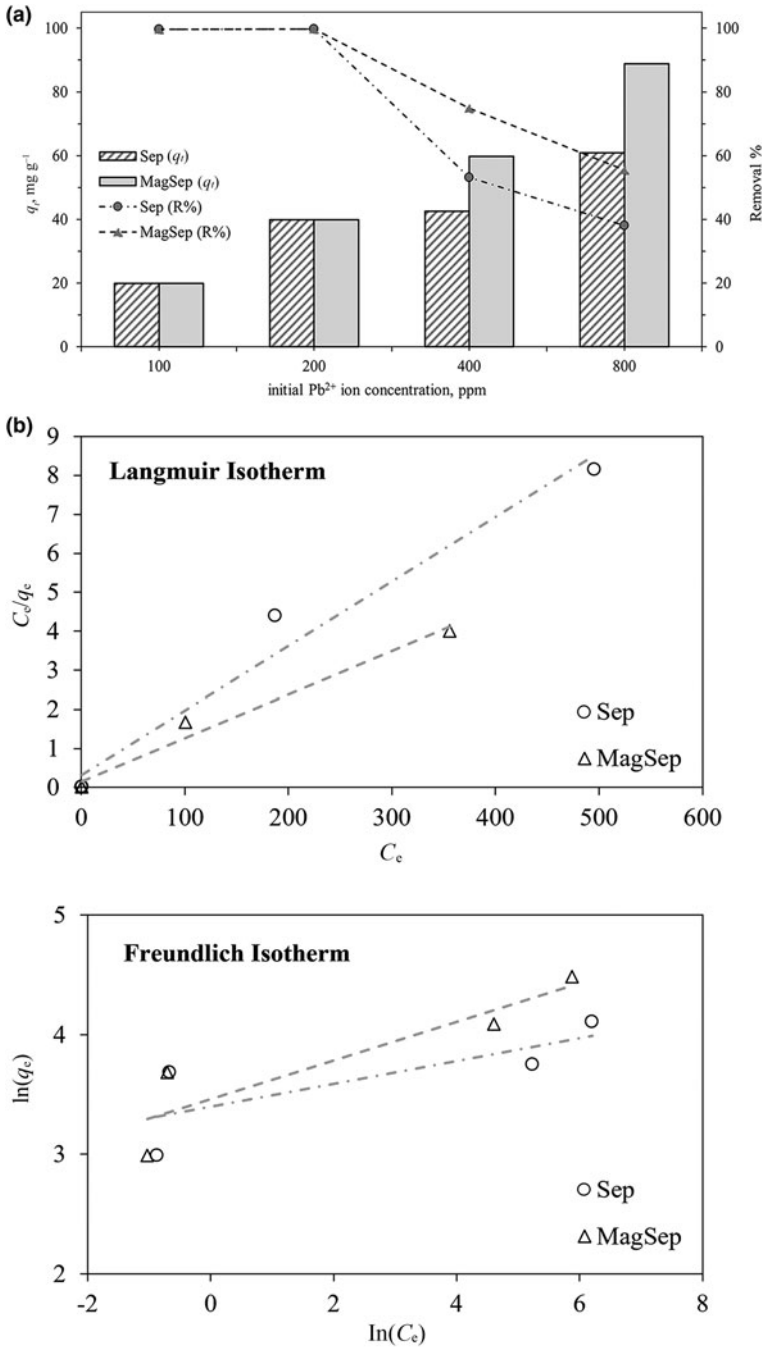

Figure 11. (a) The effect of initial Pb^{2+} concentration on the adsorption of Pb^{2+} by the sepiolite samples (pH = 7, contact time = 120 min, adsorbent dosage = 5 g L^{-1}, temperature = 25°C, initial concentration of Pb^{2+} = 400 ppm, shaking rate = 75 rpm) and (b) the adsorption isotherm models.

Table 5. Isotherm models, model constants and coefficients of correlation (R^2) for the adsorption of Pb^{2+} ions on Sep and MagSep.

Isotherm model		Model constants[a]	Sep	MagSep
Langmuir	Non-linear equation $q_e = \frac{q_m K_L C_e}{1+K_L C_e}$	q_m (mg g^{-1})	60.6	90.1
		K_L (L mg^{-1})	0.052	0.069
	Linear equation $\frac{C_e}{q_e} = \frac{1}{K_L q_m} + \frac{C_e}{q_m}$	R^2	0.9718	0.9795
Freundlich	Non-linear equation $q_e = K_F C_e^{1/n}$	n	10.4	6.2
		$K_F\left(\text{mg}^{(1-\frac{1}{n})} \times \frac{L^{\frac{1}{n}}}{g}\right)$	29.88	31.83
	Linear equation $\ln(q_e) = \ln(K_F) + \frac{\ln(C_e)}{n}$	R^2	0.5965	0.8155

[a]q_m is the maximum adsorption capacity of the adsorbents, K_L and K_F are the adsorption coefficients and n is the Freundlich constant.

plane vibrations (Eren & Gumus, 2011; Hannachi *et al.*, 2013; Kushwaha *et al.*, 2019). The intense band at 2356 cm^{-1} in the spectra of Sep and MagSep indicates that a chemical interaction occurred on the sepiolite surface during the Pb^{2+} adsorption process. In addition, the shift in the 1660 cm^{-1} (Sep) and 1654 cm^{-1} (MagSep) bands before adsorption to 1647 cm^{-1} together with the disappearance of the 1460 cm^{-1} (Sep) and 1416 cm^{-1} (MagSep) bands after adsorption demonstrate the decrease of H_2O content, being replaced by Pb^{2+} ions. The disappearance of the 690 cm^{-1} bands also demonstrate the interaction of Pb^{2+} with the Mg–OH bond (Eren & Gumus, 2011). Hence, all of these changes in the FTIR spectra are indicators of Pb^{2+} adsorption on the sepiolite samples, forming sepiolite–Pb covalent bonds.

https://doi.org/10.1180/clm.2023.24 Published online by Cambridge University Press

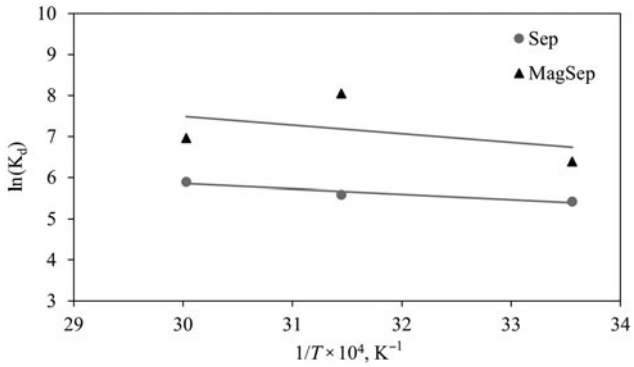

Figure 12. $\ln(K_d)$ as a function of the 1/*T* graph for the adsorption of Pb^{2+} ions by the sepiolite samples (pH = 7, contact time = 120 min, adsorbent dosage = 5 g L^{-1}, initial Pb^{2+} ion concentration = 400 mg L^{-1}, shaking rate = 75 rpm).

Table 6. Thermodynamic parameters of the adsorption of Pb^{2+} ions by Sep and MagSep.

			$\Delta G°$ (kJ mol^{-1})		
	$\Delta H°$ (kJ mol^{-1})	$\Delta S°$ (J mol^{-1} K^{-1})	298 K	318 K	333 K
Sep	10.68	80.66	−13.46	−14.79	−16.32
MagSep	15.46	106.42	−15.84	−19.53	−19.28

The SEM images of the Pb-adsorbed sepiolite samples (Fig. 3) show that the surface structure of the samples was not altered by the adsorption process. The presence of Pb^{2+} on Sep (15.36%) and MagSep (21.89%) was also verified by the elemental analysis and distribution (Fig. 4).

Conclusion

The results of this study demonstrate the potential of Sep (Eskişehir, Türkiye) and MagSep as effective, environmentally friendly adsorbents for the removal of Pb^{2+} ions from aqueous solutions. The characterization of MagSep showed that iron was incorporated into the sepiolite structure through the formation of covalent bonds. The results also illustrated that MagSep had a greater adsorption capacity for Pb^{2+} ions compared to Sep under all experimental conditions due to the high affinity of iron oxide for lead ions. Therefore, MagSep can be termed an advanced adsorbent derived from the sepiolite mineral.

The adsorption of lead on the sepiolite samples conformed to the pseudo-second-order kinetic model. The adsorption isotherm fit the Langmuir model, with monolayer adsorption capacities of 60.6 and 90.1 mg g^{-1} for Sep and MagSep, respectively. The thermodynamic parameters showed that the adsorption of Pb^{2+} on the sepiolite samples was endothermic ($\Delta H° > 0$) and adsorption occurred spontaneously ($\Delta G° < 0$). Pb^{2+} was adsorbed successfully on the sepiolite samples, as determined from the XRF, FTIR and SEM-EDS analyses. The results revealed that MagSep can be considered to be a potentially better adsorbent than Sep for Pb^{2+} remediation from aqueous solutions, and with the use of an external magnetic field it can be separated easily from aqueous solutions without releasing extra toxic pollutants into the environment. It can therefore be recommended that the use of MagSep prepared from Eskişehir sepiolite be further investigated in terms of its adsorption capacity regarding other heavy metals.

Acknowledgements. The authors thank Prof Dr Yusuf Kağan Kadıoğlu for supplying the raw sepiolite samples, Earth Sciences Application and Research Center (YEBİM) at Ankara University for the XRD, XRF and ICP-OES analysis support, the Institute of Nuclear Sciences at Ankara University for SEM-EDS analyses, Prof Dr Hande Çelebi at Eskisehir Technical University for the FTIR analysis support, Middle East Technical University (METU) Central Laboratory for the ζ-potential, VSM and BET analysis support and Superconductor Technologies Application and Research Center at Ankara University for the particle-size analysis support and for providing the permanent magnet.

Availability of data and materials. Available upon request.

Financial support. This study was partially supported by Ankara University *via* project number BAP-21L0405003.

Competing interest. The authors declare none.

Ethical standards. None.

Author contributions. Conceptualization: G.Ö. Çakal; Methodology: G.Ö. Çakal; Formal analysis and investigation: O. Uygun, A. Murat; Writing – original draft preparation: O. Uygun, A. Murat, G.Ö. Çakal; Writing – review and editing: G.Ö. Çakal; Funding acquisition: G.Ö. Çakal; Supervision: G.Ö. Çakal.

References

Al-Degs Y.S., Tutunji M.F. & Baker H.M. (2003) Isothermal and kinetic adsorption behaviour of Pb^{2+} ions on natural silicate minerals. *Clay Minerals*, **38**, 501–509.

Ahribesh A.A., Lazarević S., Janković-Častvan I., Jokić B., Spasojević V., Radetić T. *et al.* (2017) Influence of the synthesis parameters on the properties of the sepiolite-based magnetic adsorbents. *Powder Technology*, **305**, 260–269.

ASTM 4646-03 (2004) Standard Test Method for 24-h Batch-Type Measurement of Contaminant Sorption by Soils and Sediments. Retrieved from https://www.astm.org/d4646-16.html

Bektaş N., Ağım B. & Kara S. (2004) Kinetic and equilibrium studies in removing lead ions from aqueous solutions by natural sepiolite. *Journal of Hazardous Materials*, **112**, 115–122.

Bhattacharya K., Parasar D., Mondal B. & Deb P. (2015) Mesoporous magnetic secondary nanostructures as versatile adsorbent for efficient scavenging of heavy metals. *Scientific Reports*, **5**, 1–9.

Brigatti M., Medici L. & Poppi L. (1996) Sepiolite and industrial waste-water purification: removal of Zn^{2+} and Pb^{2+} from aqueous solutions. *Applied Clay Science*, **11**, 43–54.

Christidis G.E. (2011) Industrial clays. *European Mineralogical Union Notes in Mineralogy*, **9**, 341–414.

Collin M.S., Venkatraman S.K., Vijayakumar N., Kanimozhi V., Arbaaz S. M., Stacey R.G.S. *et al.* (2022) Bioaccumulation of lead (Pb) and its effects on human: a review. *Journal of Hazardous Materials Advances*, **7**, 100094.

Çoruh S., Geyikçi F. & Elevli S. (2011) Adsorption of neutral red dye from an aqueous solution onto natural sepiolite using full factorial design. *Clays and Clay Minerals*, **59**, 617–625.

Deng H., Tu Y., Wang H., Wang Z., Li Y., Chai L. *et al.* (2022) Environmental behavior, human health effect, and pollution control of heavy metal(loid)s toward full life cycle processes. *Eco-Environment & Health*, **1**, 229–243.

Dettori M., Arghittu A., Deiana G., Castiglia P. & Azara A. (2022) The revised European Directive 2020/2184 on the quality of water intended for human consumption. A step forward in risk assessment, consumer safety and informative communication. *Environmental Research*, **209**, 112773.

Doğan M., Türkyilmaz A., Alkan M. & Demirbaş Ö. (2009) Adsorption of copper (II) ions onto sepiolite and electrokinetic properties. *Desalination*, **238**, 257–270.

Doğan M., Turhan Y., Alkan M., Namli H., Turan P. & Demirbaş Ö. (2008) Functionalized sepiolite for heavy metal ions adsorption. *Desalination*, **230**, 248–268.

Erdoğan B. & Esenli F. (2021) Sepiolite as an efficient adsorbent for ethylene gas. *Clay Minerals*, **56**, 222–228.

Eren E. & Gumus H. (2011) Characterization of the structural properties and Pb(II) adsorption behavior of iron oxide coated sepiolite. *Desalination*, **273**, 276–284.

EU (2020) Directive (EU) 2020/2184 on the quality of water intended for human consumption (recast). Retrieved from https://www.fao.org/faolex/results/details/en/c/LEX-FAOC201243/

Fayazi M., Afzali D., Ghanei-Motlagh R. & Iraji A. (2019) Synthesis of novel sepiolite–iron oxide–manganese dioxide nanocomposite and application for lead(II) removal from aqueous solutions. *Environmental Science and Pollution Research*, **26**, 18893–18903.

Fei Y. & Hu Y.H. (2022) Design, synthesis, and performance of adsorbents for heavy metal removal from wastewater: a review. *Journal of Materials Chemistry A*, **10**, 1047–1085.

Fei Y. & Hu Y.H. (2023) Recent progress in removal of heavy metals from wastewater: a comprehensive review. *Chemosphere*, **335**, 139077.

González-Santamaría D.E., López E., Ruiz A., Fernández R., Ortega A. & Cuevas J. (2017) Adsorption of phenanthrene by stevensite and sepiolite. *Clay Minerals*, **52**, 341–350.

González Vázquez O.F., del Moreno Virgen M., Hernández Montoya V., Tovar Gómez R., Alcántara Flores J.L., Pérez Cruz M.A. & Montes Morán M.A. (2016) Adsorption of heavy metals in the presence of a magnetic field on adsorbents with different magnetic properties. *Industrial & Engineering Chemistry Research*, **55**, 9323–9331.

Hannachi Y., Homri T. & Boubaker T. (2013) Utilization of Tunisian bentonite as ion-exchange and sorbent material in the removal of lead from aqueous solutions. *The Holistic Approach to Environment*, **3**, 123–140.

Huang Y., Wang W., Feng Q. & Dong F. (2017) Preparation of magnetic clinoptilolite/$CoFe_2O_4$ composites for removal of Sr^{2+} from aqueous solutions: kinetic, equilibrium, and thermodynamic studies. *Journal of Saudi Chemical Society*, **21**, 58–66.

Jaishankar M., Tseten T., Anbalagan N., Mathew B.B. & Beeregowda K.N. (2014) Toxicity, mechanism and health effects of some heavy metals. *Interdisciplinary Toxicology*, **7**, 60–72.

Kara M., Yuzer H., Sabah E. & Celik M. (2003) Adsorption of cobalt from aqueous solutions onto sepiolite. *Water Research*, **37**, 224–232.

Kıpçak İ., Kurtaran Ersal E. & Özdemir M. (2020) Adsorptive removal of Ni^{2+} ions from aqueous solutions by nodular sepiolite (meerschaum) and industrial sepiolite samples from Eskişehir, Turkey. *Clays and Clay Minerals*, **68**, 220–236.

Kocaoba S. (2009) Adsorption of Cd(II), Cr(III) and Mn(II) on natural sepiolite. *Desalination*, **244**, 24–30.

Kumar V., Dwivedi S. & Oh S. (2022) A critical review on lead removal from industrial wastewater: recent advances and future outlook. *Journal of Water Process Engineering*, **45**, 102518.

Kushwaha A., Rani R. & Patra J.K. (2019) Adsorption kinetics and molecular interactions of lead [Pb(II)] with natural clay and humic acid. *International Journal of Environmental Science and Technology*, **17**, 1325–1336.

Lazarević S., Janković-Častvan I., Djokić V., Radovanović Z., Janaćković D. & Petrović R. (2010) Iron-modified sepiolite for Ni^{2+} sorption from aqueous solution: an equilibrium, kinetic, and thermodynamic study. *Journal of Chemical and Engineering Data*, **55**, 5681–5689.

Lazarević S., Janković-Častvan I., Jovanović D., Milonjić S., Janaćković D. & Petrović R. (2007) Adsorption of Pb^{2+}, Cd^{2+} and Sr^{2+} ions onto natural and acid-activated sepiolites. *Applied Clay Science*, **37**, 47–57.

Lehto J. & Hou X., editors (2010) *Chemistry and Analysis of Radionuclides: Laboratory Techniques and Methodology*. Wiley-VCH Verlag GmbH & Co. KGaA, Weinheim, Germany, 429 pp.

Liang X., Xu Y., Wang L., Sun Y., Lin D., Sun Y. *et al.* (2013) Sorption of Pb^{2+} on mercapto functionalized sepiolite. *Chemosphere*, **90**, 548–555.

Madejová J., Gates W.P. & Petit S. (2017) IR spectra of clay minerals. Pp. 107–149 in: *Developments in Clay Science*, Vol 8 (W.P. Gates, J.T. Kloprogge, J. Madejová & F. Bergaya, editors). Elsevier, Amsterdam, The Netherlands.

Mahmoud M.R., Rashad G.M., Metwally E., Saad E.A. & Elewa A. M. (2017) Adsorptive removal of $^{134}Cs^{+}$, $^{60}Co^{2+}$ and $^{152+154}Eu^{3+}$ radionuclides from aqueous solutions using sepiolite: single and multi-component systems. *Applied Clay Science*, **141**, 72–80.

Mao X., Liu H., Chu Z., Chen T., Zou X., Chen D. *et al.* (2023) Adsorption of lead by kaolinite, montmorillonite, goethite and ferrihydrite: performance and mechanisms based on quantitative analysis. *Clay Minerals*, **57**, 230–240.

Mitra S., Chakraborty A.J., Tareq A.M., Emran T.B., Nainu F., Khusro A. *et al.* (2022) Impact of heavy metals on the environment and human health: novel therapeutic insights to counter the toxicity. *Journal of King Saud University – Science*, **34**, 101865.

Novikau R. & Lujaniene G. (2022) Adsorption behaviour of pollutants: heavy metals, radionuclides, organic pollutants, on clays and their minerals (raw, modified and treated): a review. *Journal of Environmental Management*, **309**, 114685.

Otunola B.O. & Ololade O.O. (2020) A review on the application of clay minerals as heavy metal adsorbents for remediation purposes. *Environmental Technology & Innovation*, **18**, 100692.

OIK (2018) *Report No: 822*. Mining Policies Special Expertise Commission, Republic of Turkey Ministry of Development, Ankara, Türkiye.

Raj K. & Das A.P. (2023) Lead pollution: impact on environment and human health and approach for a sustainable solution. *Environmental Chemistry and Ecotoxicology*, **5**, 79–85.

Rajendran S., Priya A., Senthil Kumar P., Hoang T.K., Sekar K., Chong K.Y. *et al.* (2022) A critical and recent developments on adsorption technique for removal of heavy metals from wastewater – a review. *Chemosphere*, **303**, 135146.

Sasidharan R. & Kumar A. (2022) Magnetic adsorbent developed with alkali–thermal pretreated biogas slurry solids for the removal of heavy metals: optimization, kinetic, and equilibrium study. *Environmental Science and Pollution Research*, **29**, 30217–30232.

Sharifipour F., Hojati S., Landi A. & Faz Cano A. (2015) Kinetics and thermodynamics of lead adsorption from aqueous solutions onto Iranian sepiolite and zeolite. *International Journal of Environmental Research*, **9**, 1001–1010.

Tabak A., Eren E., Afsin B. & Caglar B. (2009) Determination of adsorptive properties of a Turkish sepiolite for removal of Reactive Blue 15 anionic dye from aqueous solutions. *Journal of Hazardous Materials*, **161**, 1087–1094.

Tamjidi S., Esmaeili H. & Moghadas B.K. (2019) Application of magnetic adsorbents for removal of heavy metals from wastewater: a review study. *Materials Research Express*, **6**, 102004.

Tartaglione G., Tabuani D. & Camino G. (2008) Thermal and morphological characterisation of organically modified sepiolite. *Microporous and Mesoporous Materials*, **107**, 161–168.

Uddin M.K. (2017) A review on the adsorption of heavy metals by clay minerals, with special focus on the past decade. *Chemical Engineering Journal*, **308**, 438–462.

Uygun O., Güven R. & Çakal G.Ö. (2023) Adsorptive removal of stable and radioactive Pb(II) isotopes from aqueous solution using bentonite, zeolite, and perlite: characterization, isotherm, thermodynamic studies. *Clay Minerals* (in press).

Wang K., Zhang F., Xu K., Che Y., Qi M. & Song C. (2023) Modified magnetic chitosan materials for heavy metal adsorption: a review. *RSC Advances*, **13**, 6713–6736.

WHO (2017) *Guidelines for Drinking-Water Quality: 4th Edition Incorporating the First Addendum*. WHO Press, Geneva, Switzerland, 631 pp.

Yu S., Zhai L., Zhong S., Qiu Y., Cheng L. & Ren X. (2016) Synthesis and structural characterization of magnetite/sepiolite composite and its sorptive properties for Co(II) and Cd(II). *Journal of the Taiwan Institute of Chemical Engineers*, **59**, 221–228.

Zhou J., Wang Z., Alcântara A.C.S. & Ding Y. (2023) Study of the adsorption mechanisms of NH_3, H_2S and SO_2 on sepiolite using molecular dynamics simulations. *Clay Minerals*, **58**, 1–6.

https://doi.org/10.1180/clm.2023.24 Published online by Cambridge University Press